Lei *et al. Discover Oncology* (2025) 16:1089
https://doi.org/10.1007/s12672-025-02912-6

Discover Oncology

RESEARCH Open Access

A novel cuproptosis-associated LncRNA model predicting prognostic and immunotherapy response for glioma

Bo Lei[1], Ao zhan[2], Guoliang You[1], Honggang Wu[1], Shu Chen[1], Daobao Zhang[1], Zhiye Liu[1] and Niandong Zheng[1*]

*Correspondence:
Niandong Zheng
zhengniandong123@163.com
[1]Department of Cerebrovascular Disease, People's Hospital of Leshan, Leshan 614000, PR China
[2]Department of Neurosurgery, People's Hospital of Leshan, Leshan 614000, PR China

Abstract

Recent studies have identified cuproptosis as a novel form of regulated cell death (RCD), and long non-coding RNAs (lncRNAs) have been implicated in glioma progression and prognosis. However, the role of cuproptosis-associated lncRNAs in gliomas has not been systematically assessed. In this study, data from the Cancer Genome Atlas (TCGA) and the Chinese Glioma Genome Atlas (CGGA) databases were used, and cuproptosis-related genes were obtained from previous research. Cuproptosis-associated lncRNAs were identified through co-expression network analysis, Cox regression, and Least Absolute Shrinkage and Selection Operator (LASSO). A total of 10 cuproptosis-associated lncRNAs were selected to construct a prognostic prediction model. The high-risk group was associated with poor overall survival (OS) and progression-free survival (PFS). Multivariate Cox regression, Receiver Operating Characteristic (ROC) curve analysis, C-index, and nomogram demonstrated the accuracy of the 10-lncRNA signature in predicting outcomes in glioma patients. Gene Ontology (GO), Kyoto Encyclopedia of Genes and Genomes (KEGG), and Gene Set Variation Analysis (GSVA) enrichment analyses revealed a strong association between the signature and immune response pathways. Immune cell infiltration and Single-Sample Gene Set Enrichment Analysis (ssGSEA) further confirmed that the signature is closely linked to immune responses in glioma patients. Further investigation revealed significant differences in tumor immune dysfunction and rejection (TIDE) scores and half-maximal inhibitory concentration (IC50) values for many drugs between low- and high-risk subgroups. This risk signature may serve as a prognostic tool and offer valuable insights into treatment strategies for glioma patients. Additionally, the expression levels of the 10 signature genes were validated by quantitative real-time polymerase chain reaction (qRT-PCR).

Keywords Cuproptosis, LncRNA, Immune microenvironment, Prognosis, Glioma

1 Introduction

Glioma is one of the most common and aggressive primary intracranial tumors in the nervous system [1]. According to the World Health Organization (WHO) classification, gliomas are categorized into low-grade gliomas (Grade II) and high-grade gliomas

(Grade III-IV). Grade II refers to low-grade glioma (LGG), while Grade III and Grade IV are high-grade gliomas (HGG), with Grade IV being the most aggressive, representing glioblastoma (GBM) [2, 3]. Currently, the standard treatment for gliomas includes surgical resection combined with radiotherapy and chemotherapy, primarily temozolomide [4, 5]. The median survival of patients with low-grade gliomas is approximately 5 years, while patients with glioblastoma have a survival rate of 1 to 2 years [6, 7]. Despite advances in treatment, survival rates for glioma patients have not significantly improved, mainly due to tumor proliferation, invasion, metastasis, resistance, and tumor heterogeneity [8–10]. The tumor microenvironment (TME) is one of the key factors contributing to glioma heterogeneity [11, 12]. The TME includes cancer cells and various non-tumor cells, such as pericytes, endothelial cells, and immune cells [13, 14]. Additionally, factors such as chemokines, cytokines, and growth factors secreted by cells all contribute to the formation of the TME [15, 16]. Accurately assessing the individual tumor microenvironment in glioma patients can help better predict patient risk and formulate personalized treatment plans. Although the WHO classification system is widely used for glioma typing, molecular biology advancements have improved glioma classification through the application of molecular markers, such as isocitrate dehydrogenase (IDH) mutations [17], O6-methylguanine-DNA methyltransferase (MGMT) promoter methylation [18], and 1p/19q co-deletion [19]. However, the existing classification systems sometimes fail to comprehensively reflect all biological characteristics of gliomas, highlighting the need for the development of more precise and comprehensive risk assessment models to better understand glioma heterogeneity and provide personalized treatment strategies for patients.

Resistant cell death, including accidental cell death (ACD) and regulated cell death (RCD), is a hallmark of tumor cells [20]. While ACD is uncontrollable, RCD involves regulated mechanisms, with apoptosis being the most studied. Other types of RCD include autophagy, pyroptosis, ferroptosis, and immunogenic cell death [20]. Cuproptosis, a recently discovered form of RCD, is copper-dependent and closely linked to mitochondrial respiration [21–23]. Copper binds to lipoacylated proteins in the tricarboxylic acid cycle, causing aggregation and loss of Fe-S cluster proteins, leading to proteotoxic stress and triggering cuproptosis [24]. Additionally, copper metabolism maintains cellular homeostasis and influences physiological functions [25, 26]. Copper-induced cell death occurs through pathways like ER stress, oxidative stress, autophagy, and mitophagy [27, 28]. Copper also induces necrotic apoptosis via ROS-dependent DNA damage [29] and can trigger NLRP3-dependent pyroptosis, contributing to nervous system toxicity and inflammation [30, 31]. Moreover, cuproptosis is linked to ferroptosis, a form of cell death regulated by redox reactions and metabolism, with potential for anti-tumor therapies [32, 33]. Studies have shown that cuproptosis can induce ferroptosis in nerve cells, and targeting intracellular copper may enhance tumor sensitivity to treatment [34, 35]. The interplay between copper and ferroptosis through copper-iron homeostasis modulation may also increase radiosensitivity in cancer cells [36]. However, the role of cuproptosis in gliomas remains unclear and requires further investigation.

Long non-coding RNAs (lncRNAs) are RNA transcripts longer than 200 base pairs that play important roles in various biological processes, such as cell differentiation, tumorigenesis, metastasis, immune response, and tumor drug resistance [37–39]. Recently, tumor prediction models based on multiple lncRNAs have shown greater

accuracy compared to single molecular models [40–42]. However, the value of cuproptosis-associated lncRNAs in gliomas has not been systematically evaluated.

This study identified cuproptosis-associated lncRNA signatures that are independently related to glioma prognosis, constructed and validated a novel prognostic model, calculated individualized risk scores, and further analyzed the tumor immune microenvironment and drug sensitivity in patients with different risk stratifications. The study aims to identify potential biomarkers and help predict patient prognosis to develop effective personalized treatment strategies.

2 Methods

2.1 Data collection and preprocessing

We obtained transcriptome expression profiles, clinical characterization data, mutation data, and copy number variation (CNV) data from glioma patients, including 144 GBM and 506 LGG samples, from The Cancer Genome Atlas (TCGA, https://portal.gdc.cancer.gov/) database. In addition, transcriptome expression and clinical characterization data for glioma patients in the CGGA693 and CGGA325 cohorts, comprising 388 GBM and 626 LGG samples, were downloaded from the Chinese Glioma Genome Atlas (CGGA, http://www.cgga.org.cn/index.jsp) database.

The CGGA693 cohort consists of glioma patients with a broad spectrum of molecular subtypes, including IDH wild-type and IDH-mutant gliomas, whereas the CGGA325 cohort includes a more specific subset of glioma patients with distinct clinical features, such as specific tumor grades or treatment statuses. These two cohorts were used in parallel to ensure comprehensive analysis across different clinical and molecular profiles. The specific characteristics of these cohorts, such as tumor grade, molecular subtype (e.g., IDH mutation status), and treatment status, are detailed in the original CGGA database documentation.

Additionally, we obtained transcriptome expression data of non-tumoral brain samples from the Genotype-Tissue Expression (GTEx) database (https://www.gtexportal.org), which includes tissue samples from healthy individuals. These non-tumoral brain samples served as controls to compare against glioma tissues. However, it is important to note that although GTEx provides non-tumoral brain tissue, these samples may still reflect changes due to other health conditions (such as trauma or epilepsy), which could slightly influence the gene expression profiles. Thus, while GTEx non-tumoral samples serve as a useful reference for normal brain tissue, they may not perfectly represent "normal" brain tissue in the context of glioma pathology. All data was downloaded on March 19, 2024. To facilitate subsequent analyses, we normalized the transcriptome data using transcripts per kilobase million (TPM), which accounts for both gene length and sequencing depth. Following TPM normalization, we further ensured consistency across datasets by performing quantile normalization and log transformation to address any platform-specific biases and to stabilize variance across samples [43].

The ComBat function from the SVA R package was used to correct batch effects between different datasets (TCGA, CGGA, GTEx) to reduce technical variations caused by differing sequencing platforms [44]. To assess the effectiveness of batch effect correction, we visualized the corrected data using Principal Component Analysis (PCA), ensuring that batch effects were adequately removed.

In addition to the batch effect correction, we performed additional data quality control by removing low-expression genes (genes with low variance across all samples) and identifying potential outlier samples using PCA plots (Supplementary Fig. 1). These outliers were excluded from downstream analysis to ensure that only high-quality samples were included.

By applying these rigorous QC procedures and normalization methods, we ensured the reliability and robustness of the data used in subsequent analyses.

3 Establishment of cuproptosis associated LncRNA signatures

Nineteen CRGs were obtained from previous studies (supplementary Table 1) [21, 45–48]. The maftools R package was used for Copy Number Variation (CNV) analysis of those genes [49]. The co-expression correlation analysis was performed to identify cuproptosis-associated lncRNAs (cur-lncRNAs) using limma R package ($r > 0.4$ & $P < 0.001$) [50].

4 Modeling and validation of the prognostic cuproptosis-associated LncRNA signature

Patients were randomly assigned to either a training group or a testing group in a 1:1 ratio. In the training cohort, we first performed univariate Cox regression to identify cur-lncRNAs associated with patient prognosis. LASSO-Cox regression was then used to create the cur-lncRNA signature model [51]. The best model parameters were selected via multivariate Cox regression analysis ($P < 0.05$), and risk scores for each patient were calculated using the following formula: Risk score = ∑i Coefficient(i) * Expression(i) where Coefficient represents the regression coefficient of lncRNA, and Expression represents the expression level of the candidate lncRNA. Based on the median risk score from the training cohort, all glioma patients were categorized into low-risk and high-risk subgroups. Kaplan-Meier survival analysis was performed to compare overall survival (OS) or progression-free survival (PFS) between the two subgroups across all cohorts (training, testing, and various subgroups). The correlation between the model and clinical features was evaluated using the chi-square test.

5 Construction of the nomogram

We constructed nomograms which combined risk scores with clinical factors, including type (Primary or Unprimary), grade (WHO II/III or WHO IV), gender (male or female), age, radiotherapy (no or yes), TMZ therapy (no or yes), IDH (Wildtype or Mutant), 1p19q (Non-codel or Codel), and MGMTp (un-methylated or methylated), to predict 1-, 3-, and 5- years OS. A time-dependent receiver operating characteristic (time-ROC) curve was drawn and the area under the curve (AUC) was calculated to measure the predictive power of our model [52]. The calibration curve and concordance index (C-index) showed the accuracy of the nomogram [53].

6 Principal component analysis (PCA) and enrichment pathway analysis

PCA was used on all sample to assess patterns associated with all genes, cuproptosis, all cur-lncRNAs, and cur-lncRNA signatures in our model [54]. Moreover, the differentially expressed genes (DEGs) between the low- and high-risk subgroups were identified ($|\log FC| > 1$, FDR < 0.05). Then, both Gene Ontology (GO) and Kyoto Encyclopedia

of Genes and Genomes (KEGG) analyses were performed to find significantly enriched biological processes and pathways using the clusterProfiler R package [55].

6.1 The tumor mutation burden (TMB) analysis and immune analysis

After extract the mutation data from TCGA database by Pearl programming language, the maftools R package was performed to examined and integrated TMB, and the differences in TMB between the low- and high-risk subgroups was analyzed. Then, the differences in Stromal, Immune, and ESTIMATE scores based on the ESTIMATE algorithm between the two subgroups were explored [56]. By using the limma, GSVA, and GSEABase R packages for single sample gene-set enrichment analysis (ssGSEA), we analyzed differences in 28 types of immune cell infiltration and immune-related functions between the two risk subgroups [57]. Then, heatmap was ploted to visalize the results.

7 Tumor immune dysfunction and exclusion (TIDE) score and drug sensitivity analysis

We obtained the TIDE scoring file, which includes components such as TIDE, Dysfunction, Exclusion, and Microsatellite Instability (MSI), from the TIDE website (http://tide.dfci.harvard.edu) to assess which risk subgroup in glioma shows better outcomes [58]. The TIDE score reflects the overall likelihood of a tumor responding to immune checkpoint therapy. It consists of three key components: Dysfunction, Exclusion, and MSI. Dysfunction represents the inability of T cells to effectively recognize and kill tumor cells, which can be indicative of a tumor's resistance to immune responses. Exclusion refers to the inability of immune cells to infiltrate the tumor microenvironment, often due to factors like physical barriers or immune evasion mechanisms. MSI indicates the degree of genetic instability in tumor cells, which may affect how the tumor interacts with immune surveillance. A higher TIDE score suggests a poor response to immune checkpoint therapy and may predict a worse survival outcome following immunotherapy. The risk subgroups in our study were defined based on the risk score calculated from the key genes (risk cuproptosis-lncRNAs) identified in prior analyses. Additionally, we used the pRRophetic R package to calculate the half maximal inhibitory concentration (IC50) value, which helps predict drug sensitivity in the low- and high-risk subgroups.

8 Quantitative real-time PCR

Tissue samples of 10 GBM and 10 brain tissues were obtained in the Guizhou Provincial People's Hospital for qPCR. They were approved by the Ethics Committee of Guizhou Provincial People's Hospital. All patients have written informed consents. Total RNA from tissues or cells was extracted using RNAiso Plus (TaKaRa, Beijing, China). The concentrations of these RNA samples were then measured using a spectrophotometer and cDNA were synthesized from the RNA specimens using the Primescript RT reagent Kit (TaKaRa). Amplification conditions were as follows: 95 °C for 30 s, followed by 40 cycles at 95 °C for 15 s, and 60 °C for 45 s. The relative fold changes in mRNA levels were calculated according to the relative quantification method ($2 - \Delta\Delta Ct$).

9 Results

9.1 Prognosis-Related LncRNAs with coexpression of cuproptosis

Our study found significant differences in cuproptosis genes between glioma and normal brain tissue (Fig. 1A). The investigation of CNV alterations showed that the amplification and deletions in copy number were not universally prevalent. The primary CNV deletions on genes were CDKN2A, ATP7B and DLST (Fig. 1B). Figure 1C shows the location of the copper death gene CNV alteration on the chromosome. Next, we found 336 lncRNA in glioma associated with CRGs ($|R| > 0.4$ & $P < 0.001$)). Pyecharts visualization co-expression relationship (Fig. 1D). Subsequently, 153 cur-lncRNAs were obtained by univariate cox regression analysis in the training cohort (Supplementary Fig. 2). Finally, using Lasso and multivariate Cox analysis, we identified 10 prognostic related cur-lncRNAs, including FAM66C, AC062021.1, RFPL1S, AP000439.1, SMCR5,

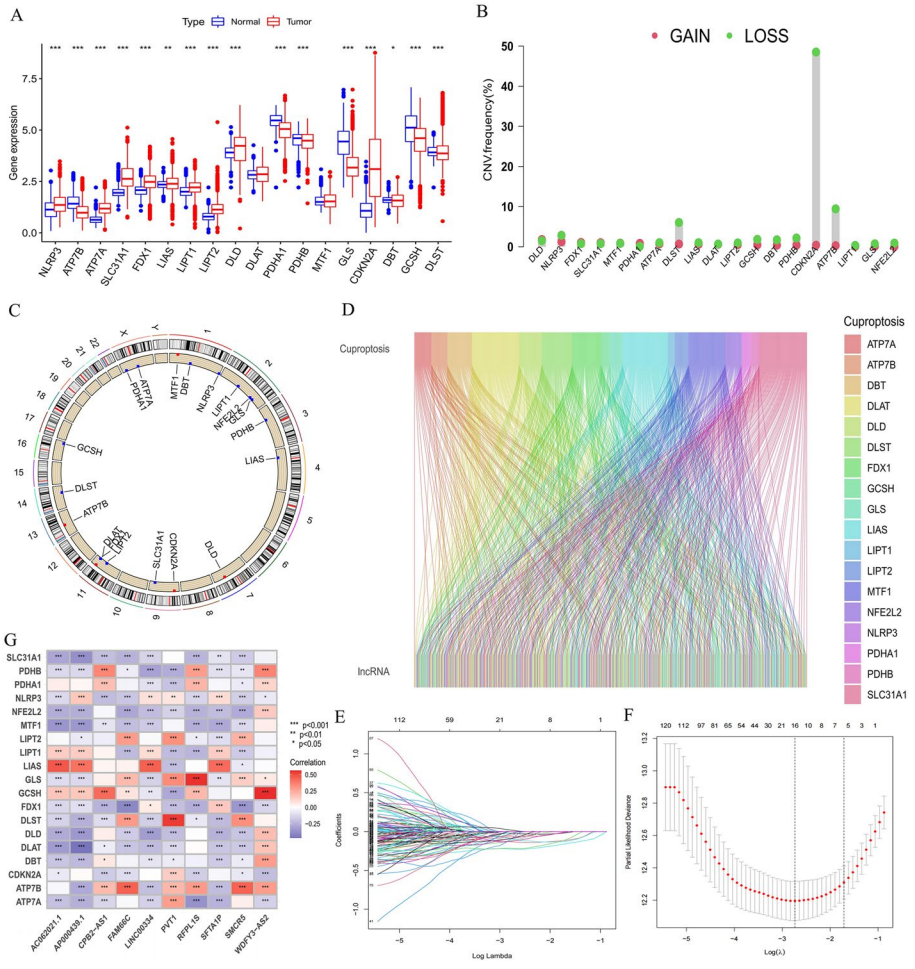

Fig. 1 Landscape of genetic and expression variation of cuproptosis-related genes in glioma and Establishment of Cuproptosis-associated lncRNA signatures. (A) Cuproptosis-related genes expressed in tumor and normal samples. (B) The frequency of CNV variation of Cuproptosis-related genes in TCGA-GBM and TCGA-LGG cohorts. green dot represented deletion frequency; red dot represented amplification frequency. (C) The location of CNV alteration of Cuproptosis-related genes on 23 chromosomes using TCGA-GBM and TCGA-LGG cohorts. (D) Sankey relationship diagram showed the co-expression of cuproptosis genes and cuproptosis-associated lncRNAs. (E) Partial likelihood deviance for each independent variable. (F) LASSO regression screened of cuproptosis-related lncRNAs. Dotted vertical lines were drawn at the optimal values by using the minimum criteria (G) Correlations between cuproptosis-related genes and cuproptosis-associated lncRNAs in our risk models using Spearman analysis. Blue represented negative correlation and positive correlation with red represented positive correlation. The asterisks represented the statistical p value (*$P < 0.05$; **$P < 0.01$; ***$P < 0.001$)

LINC00334, SFTA1P, WDFY3-AS2, PVT1, and CPB2-AS1 (Fig. 1E, F; Supplementary Table 2). The correlation relationship between the CRGs and the 10 cur-lncRNAs was showed in a heatmap (Fig. 1G).

9.2 Construction of the predictive model based on cuproptosis-related LncRNA

We constructed predictive model by calculating risk score using formula: risk score = FAM66C × (−0.2834) + AC062021.1 × (−0.2339) + RFPL1S × (−0.2052) + AP000439.1 × (−0.2151) + SMCR5 × (−0.5676) + LINC00334 × (−0.4595) + SFTA1P × (−0.2462) + WDFY3-AS2 × (−0.2598) + PVT1 × (0.1411) + CPB2-AS1 × (−0.2484). KM curve showed that the prognosis of low-risk subgroup was significantly better than that of high-risk subgroup in all glioma patients, training and testing cohort (Fig. 2A-C). Most of the patients in low-risk subgroup were in survival state, while most in high-risk subgroup were in death state (Fig. 2D and Supplementary Fig. 3 A, B). In the high-risk subgroup, only PVT1 expression was low, while the other 9 prognostic-related cur-lncRNAs were all highly expressed. The opposite is true in low-risk subgroup.

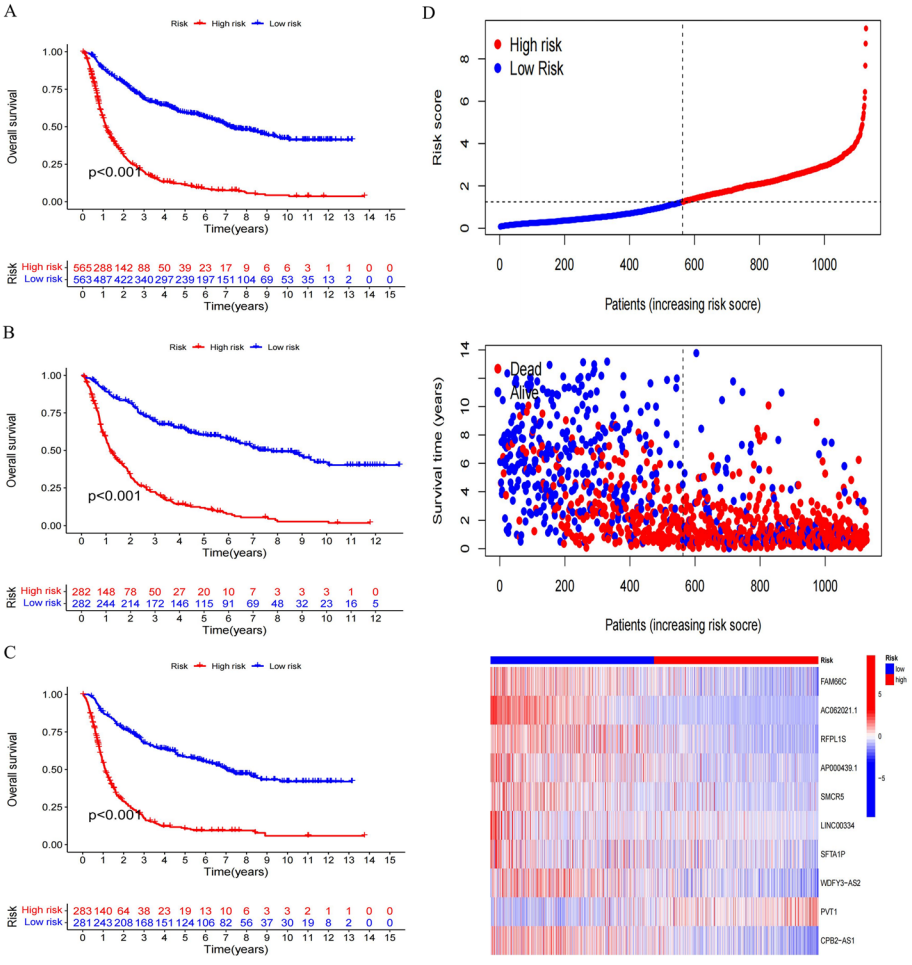

Fig. 2 Kaplan–Meier survival analyses of patients and predicting the performance of characteristics. (A-C) Survival analyses for patients high risk and low risk groups in the all cohort (A), training cohort (B) and testing cohort (C) using Kaplan-Meier curves ($P < 0.001$, Log-rank test). (D) The risk score, survival status, and expression profile of 10 cuproptosis-related lncRNAs prognostic signature in each patients in all cohort

9.3 Construction and validation of the prognostic model

In the total sample group, univariate cox regression analysis displayed that the risk score was prognostic risk factor with HR was 1.587 ($p < 0.001$) (Fig. 3A). Multivariate cox regression analysis revealed that tumor type, grade, age, TMZ therapy, 1p19q codel, MGMTp methylated, and risk score [HR = 1.308 95%CI (1.204 – 1.422), $p < 0.001$] were independent prognostic factors (Fig. 3B). In order to evaluate the predictive ability of risk score, we drew a time-dependent ROC curve, and AUC was 0.761 at 1 year, 0.837 at 2 year, and 0.858 at 5 year (Fig. 3C). In addition, we also compared the predictive ability of risk score and other clinical features. The 1-, 3-, and 5-year AUC of risk score was higher than the AUC of other clinical features (Fig. 3D-F). Furthermore, the C-index values of risk scores from 1 to 10 years were higher than those of other clinical features (Fig. 4A). Moreover, we created a nomogram according to clinical features and risk score, which can accurately predict the survival of glioma patients (Fig. 4B). Calibration curves for OS confirmed that the prediction results were in good consistency with the actual outcomes (Fig. 4C). Meanwhile, In different clinical subsets, the low-risk group still showed significantly better prognosis (Supplementary Fig. 4).

9.4 PCA and biological enrichment pathway analysis

In addition, we performed PCA to explore the distribution of patients in low- and high-risk subgroups for four expression profiles, including total genes, cuproptosis genes, cur-lncRNAs, and risk cur-lncRNAs. And the results indicated that these risk cur-lncRNAs can make a clear distinction of glioma patients and be credibly used to construct prognostic model (Fig. 5A-D). In order to detect differences between the low- and high-risk subgroups, we dentified 2007 DEGs between the two subgroups (Supplementary Table 3). GO analysis found that these DEGs enriched in regulation of trans-synaptic signaling, extracellular matrix/structure organization, synaptic membrane, endoplasmic

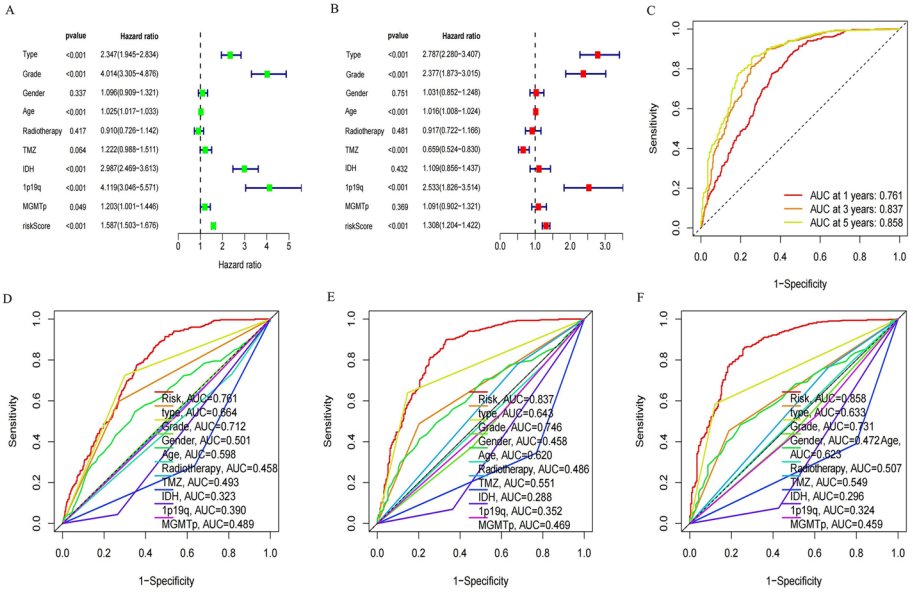

Fig. 3 The prognostic value of the signature for glioma. (A, B) The forest figure for Univariate (A) or Multivariate (B) Cox regression analysis showed that the risk score was independently associated with OS. (C) 1-, 3-, and 5-year area under the ROC curve (AUC) of risk score in the all cohort. (D-F) Prediction of 1- (D), 3- (E), and 5- (F) years ROC curves for the riskscore compared with other clinical characteristics

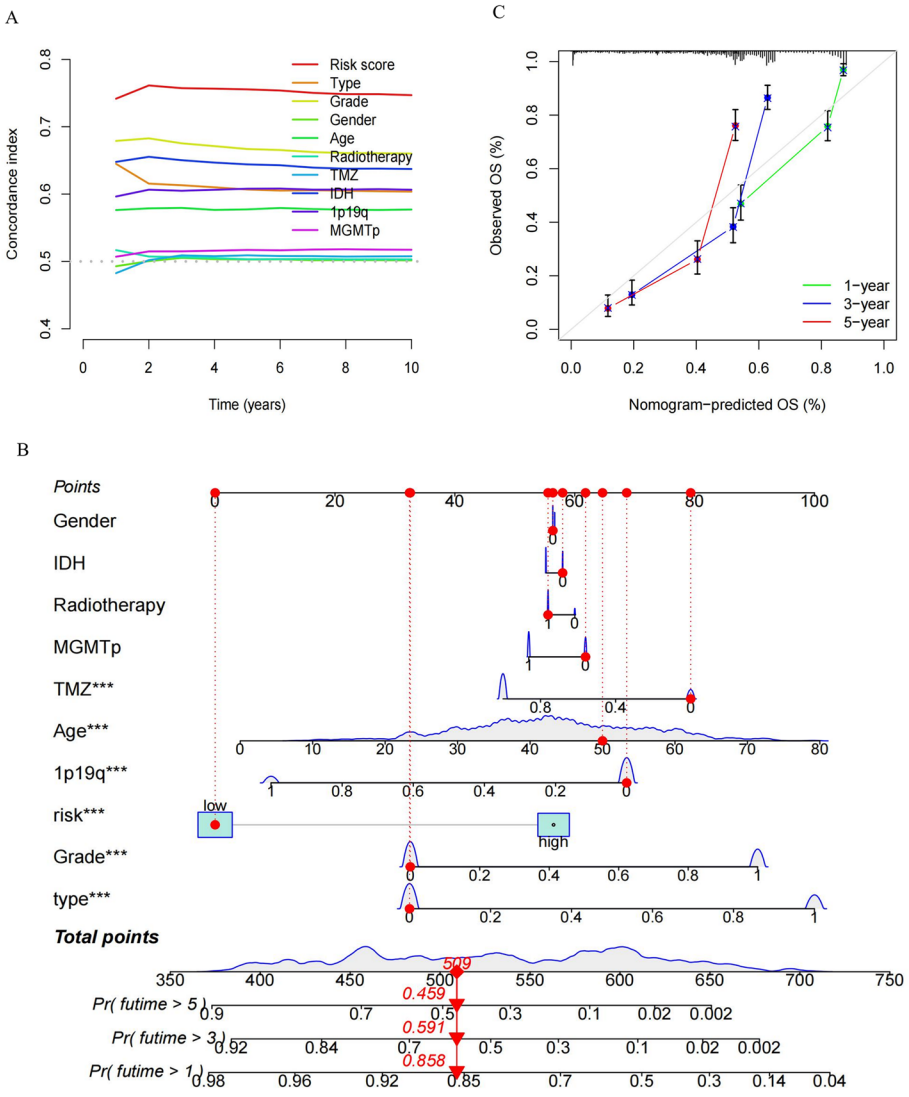

Fig. 4 Nomogram and clinical subgroups for predicting glioma outcomes. (A) C-index curve of the risk score compared with other clinical characteristics. (B) Prognostic nomogram combining clinical variables and risk scores predicts 1-, 3-, and 5-years OS in patients with glioma. (C) Calibration curves for 1, 3, and 5 years showed the agreement between actual and predicted outcomes at 1, 3, and 5 years

reticulum lumen, and glycosaminoglycan binding (Fig. 5E). KEGG analysis revealed that ECM-receptor interaction, Phagosome, Focal adhesion, and Proteoglycans in cancer, were mainly enriched (Fig. 5F). Furthermore, the heatmap showed that immuno-related functions were significantly different in two risk groups, and all immune functions were significantly more active in the high-risk subgroup (Fig. 6A). In addition to VTCN1 expression, the rest of checkpoint genes and Chemokines showed significant differences in two risk groups (Fig. 6B). Besides, vioplot showed that stromal scores, immune scores and ESTIMATE scores were significant higher in high-risk group (Fig. 6C). This results obviously suggested that there is a significant correlation between TME and risk score. Based on ssGSEA algorithms, the boxplot showed the more infiltration of immune cell populations in high-risk subgroup (Fig. 6D).

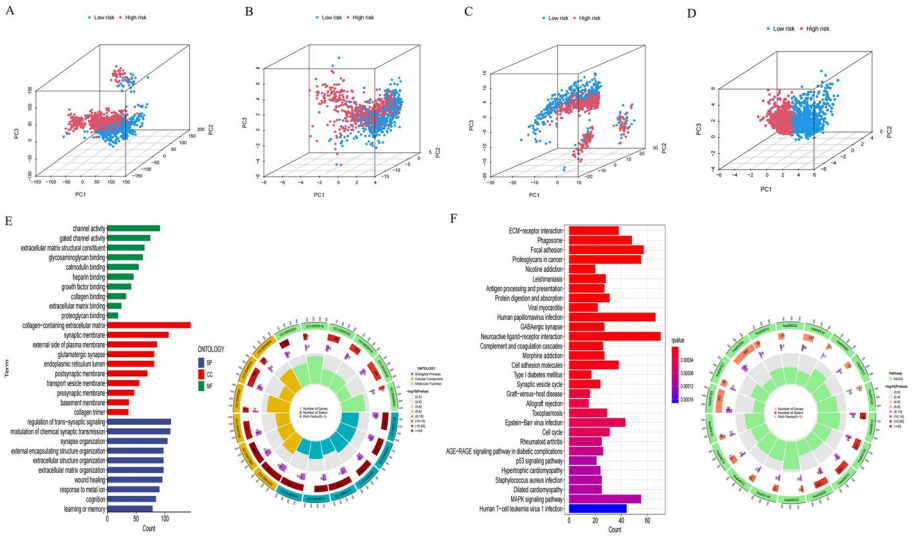

Fig. 5 PCA in both groups of patients and GO and KEGG analysis. (A-D) PCA analysis depicted the distribution of patients based on all genes (A), cuproptosis (B), all cuproptosis-associated lncRNAs (C), and Cuproptosis-associated lncRNA signatures in our model (D). (E) Gene Ontology (GO) enrichment analysis of the different expressed genes between two risk groups demonstrated the richness of molecular biological processes (BP), cellular components (CC), and molecular functions (MF). (F) KEGG enrichment analysis of the different expressed genes between two risk groups

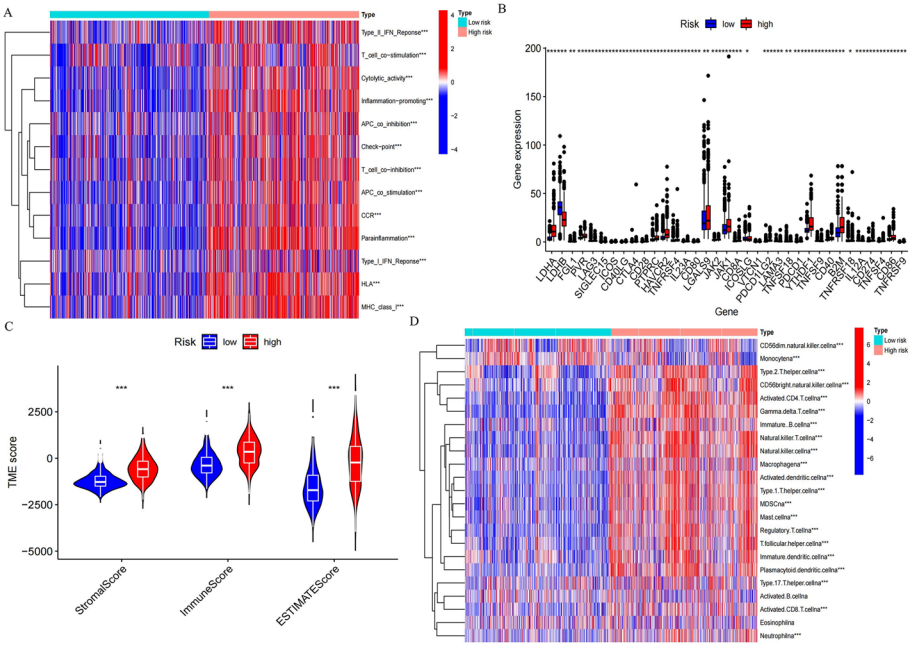

Fig. 6 Differences in the tumor immune microenvironment between the low- and high-risk groups. (A) ssGSEA scores of Immune-related functions in the low- and high-risk groups. (B) Immune checkpoint genes and Chemokines expression in the low- and high-risk groups. (C) Violin plots comparing StromalScore, ImmuneScore and ESTIMATEScore between the low- and high-risk groups, respectively. (D) The infiltration of 28 immune cells between low- and high-risk groups. The asterisks represented the statistical p value (*$P < 0.05$; **$P < 0.01$; ***$P < 0.001$)

9.5 TMB analysis and therapeutic drug sensitivity

The somatic mutation data was analyzed to observe changes in mutations in the different risk subgroups. In low-risk subgroup, EGFR (36%), SPTA1 (29%), PTEN (14%), TP53 (14%), MUC16 (14%), FLG (7%), PIK3R1 (7%), PCLO (7%), and IDH1 (7%) were top 9 mutated genes, while in high-risk subgroup, TP53 (33%), PTEN (29%), TTN (27%), EGFR (21%), MUC16 (14%), NF1 (10%), PIK3CA (10%), FLG (9%), RYR2 (9%), SPTA1 (9%) were top 10 mutated genes (Fig. 7A, B). But, difference of TMB between the two subgroups was no significant. In addition, the high TMB group had a better prognosis than the low TMB group, but there was no significant difference in prognosis between the groups after adding risk score(Fig. 7C-E). In addition, TIDE algorithm was used to estimate the diference in sensitivity to immune checkpoint therapy between two risk subgroups. The TIDE score, Exclusion score, and Dysfunction score, was higher in high-risk subgroup, while MSI was higher in low-risk subgroup (Fig. 7F). To further explore the applicability of these findings, we conducted a subgroup analysis for both IDH-wildtype and IDH-mutant gliomas. The results showed that, regardless of whether the gliomas were IDH-wildtype or IDH-mutant, the findings remained consistent with the

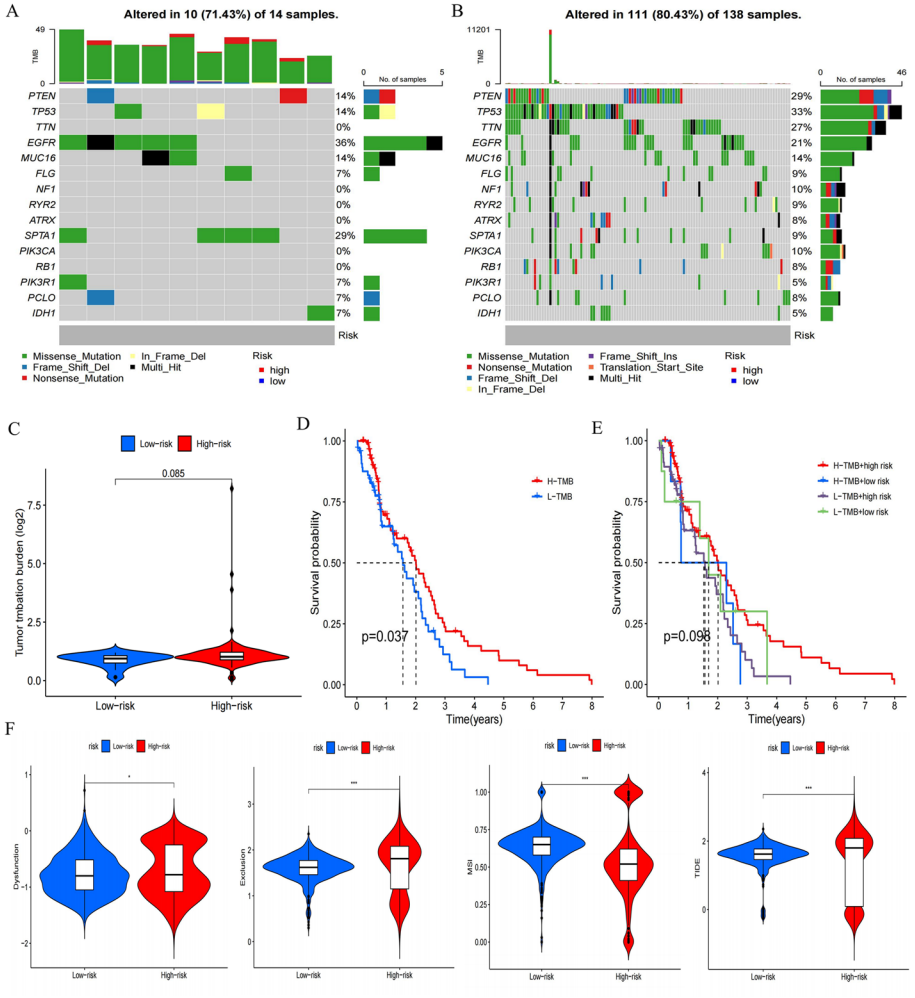

Fig. 7 TMB, TIDE, and Chemotherapeutic Sensitivity. (A, B) Waterfall plots of top 15 mutation genes in glioma for the low-risk (A) and high-risk groups (B). (C) TMB between the low-risk and high-risk groups. (D) Survival curves between the high- and low-TMB groups. (E) Survival curves for the high-TMB and low-TMB groups in GBM and a combined risk score. (F) TIDE, Dysfunction, Exclusion and MSI scores between the low- and high-risk groups

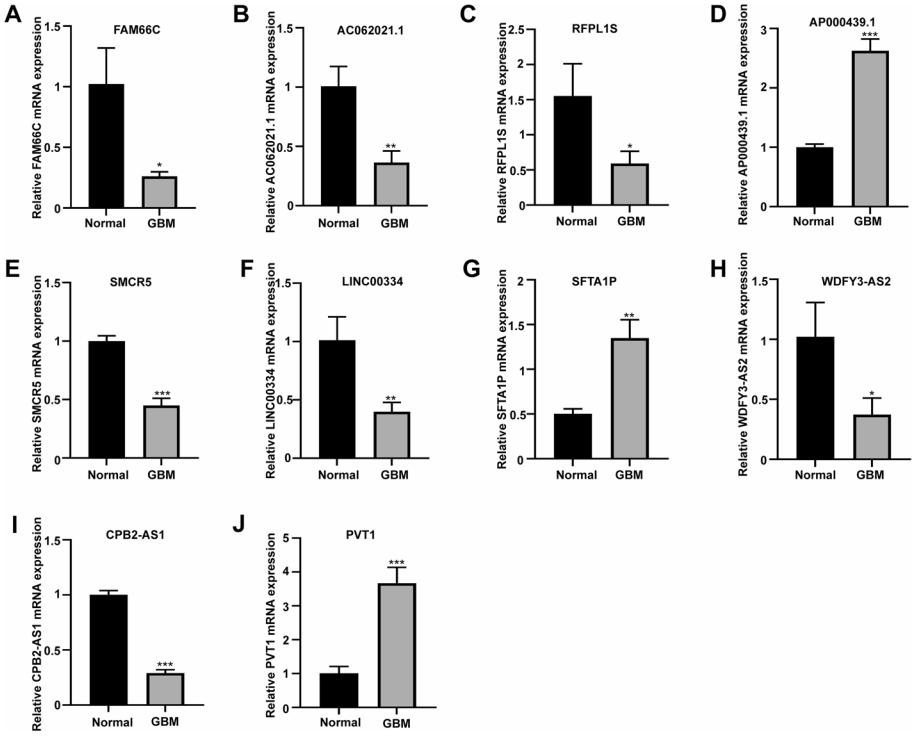

Fig. 8 q-PCR analysis of 10 lncRNAs in glioma tissues in GBM and normal brain tissues. (A) FAM66C expression was lower in GBM tissues (GBM) compared to brain tissues (Normal). (B) AC062021.1 expression was lower in GBM compared to Normal. (C) RFPL1S expression was lower in GBM compared to Normal. (D) AP000439.1 expression was lower in GBM compared to Normal. (E) SMCR5 expression was higher in GBM compared to Normal. (F) LINC00334 expression was higher in GBM compared to Normal. (G) SFTA1P expression was higher in GBM compared to Normal. (H) WDFY3-AS2 expression was higher in GBM compared to Normal. (I) CPB2-AS1 expression was higher in GBM compared to Normal. (J) PVT1 expression was higher in GBM compared to Normal. (* $P < 0.05$, ** $P < 0.01$, *** $P < 0.001$)

overall results, supporting the robustness of our model across different glioma subtypes (Supplementary Fig. 5). The drug sensitivity analysis showed that the many drugs' IC50 values were significantly different in low- and high-risk subgroups, indicating that the sensitive drugs of each subgroup were different (Supplementary Fig. 6, 7).

9.6 The expression of 11 signatures in GBM

We examined mRNA levels of 10 signatures in GBM tissues compared to normal brain tissues. FAM66C, AC062021.1, RFPL1S, SMCR5, LINC00334, and CPB2-AS1 expression was higher in GBM compared to normal, while AP000439.1, SFTA1P and PVT1 expression was lower in GBM compared to normal, which were consistent with the results of our bioinformatics analysis (Fig. 8).

10 Discussion

Gliomas are the most common central nervous system tumors and are classified into different grades based on their pathological features. Despite significant advancements in the diagnosis and treatment of gliomas, the heterogeneity and aggressiveness of these tumors continue to present considerable challenges. The molecular heterogeneity of gliomas is a fundamental factor contributing to their complexity, which complicates treatment strategies [59]. Over the past few years, molecular subtyping has emerged as a strong predictor of prognosis and treatment response in glioma patients [60–63].

However, the longstanding WHO classification system still has limitations in accurately predicting clinical outcomes. Identifying novel biomarkers, particularly through multi-biomarker approaches to construct predictive models, holds significant promise for improving prognostic accuracy and developing more tailored treatment strategies for glioma patients.

Programmed cell death (PCD) plays a crucial role in glioma initiation, progression, and metastasis [64, 65]. PCD encompasses various regulated cell death pathways, including apoptosis, ferroptosis, autophagy, necrosis, and pyroptosis [66, 67]. The relationship between PCD and resistance to immunotherapy, as well as the immunosuppressive tumor microenvironment (TME), remains complex and poorly understood [64]. Recently, Tsvetkov et al. proposed cuproptosis as a novel form of PCD linked to mitochondrial respiration and copper metabolism [21]. Copper, an essential metal, is involved in various cellular processes; however, its dysregulation can lead to cellular toxicity and death [68, 69]. Studies have shown that copper can inhibit glioma cell growth, and copper ionophores, such as Disulfiram (DSF), have been tested in clinical trials as potential therapeutic agents for glioma treatment [70–72]. Despite this progress, the role of cuproptosis in glioma remains incompletely understood.

In the present study, we identified 19 cuproptosis-related genes and 336 long non-coding RNAs (lncRNAs) associated with cuproptosis. Using Lasso-Cox regression, we identified 10 independent prognostic cuproptosis-related lncRNAs: FAM66C, AC062021.1, RFPL1S, AP000439.1, SMCR5, LINC00334, SFTA1P, WDFY3-AS2, PVT1, and CPB2-AS1. Several of these lncRNAs have been implicated in various cancers. For example, FAM66C inhibits glioma cell proliferation through the Hippo pathway [73–76], while AC062021.1 is associated with poor prognosis in glioma [77]. RFPL1S has shown predictive value in melanoma models [78], and SMCR5 is linked to carboplatin resistance in ovarian cancer [79]. SFTA1P regulates PCD and may serve as a target for cancer therapy [80], while WDFY3-AS2 and CPB2-AS1 are associated with prognosis in glioma and ferroptosis regulation [81, 82]. PVT1 is involved in gemcitabine resistance and glioma stemness [83, 84], and its expression is higher in GBM than in LGG, correlating with poor prognosis [81, 85]. These findings, along with our own, suggest that cuproptosis-related lncRNAs play pivotal roles in glioma progression.While these associations support the biological relevance of our findings, it is important to note that they are correlative, and further functional validation is needed to elucidate their mechanistic roles in cuproptosis and glioma biology. However, further experimental validation is required to fully elucidate their mechanisms and assess their potential as therapeutic targets. In addition to identifying prognostic lncRNAs, we applied the TIDE algorithm to investigate immune response differences between low- and high-risk subgroups. Our analysis revealed significant variations in the sensitivity of these subgroups to immune checkpoint therapy. Specifically, the low-risk subgroup exhibited greater sensitivity to immunotherapy, while the high-risk subgroup demonstrated resistance. This discrepancy may be linked to distinct features in the TME of these two subgroups. The higher TIDE scores in the high-risk subgroup suggest immune dysfunction and exclusion, both of which are commonly associated with resistance to immune checkpoint inhibitors. In contrast, the low-risk subgroup showed a more robust immune response, likely contributing to its enhanced sensitivity to immunotherapy. These findings suggest that risk stratification based on

cuproptosis-related lncRNAs could serve as an effective biomarker for predicting the efficacy of immunotherapy in glioma patients.

In our study, we systematically identified 19 cuproptosis-related genes and 336 associated long non-coding RNAs (lncRNAs). Using Lasso-Cox regression analysis, we further refined a 10-lncRNA signature—including FAM66C, AC062021.1, RFPL1S, AP000439.1, SMCR5, LINC00334, SFTA1P, WDFY3-AS2, PVT1, and CPB2-AS1—that was associated with patient prognosis. Some of these lncRNAs have been reported in previous cancer studies. For instance, FAM66C has been implicated in glioma cell proliferation via the Hippo pathway [73], while AC062021.1 is linked to poor glioma prognosis [77]. RFPL1S and SMCR5 have been associated with outcomes in melanoma and ovarian cancer, respectively [78, 79], and SFTA1P has been noted to regulate PCD and could potentially serve as a therapeutic target [80]. Other components of our signature, such as WDFY3-AS2, CPB2-AS1, and PVT1, have also been associated with glioma progression or drug resistance [81–85]. While these associations support the biological relevance of our findings, it is important to note that they are correlative, and further functional validation is needed to elucidate their mechanistic roles in cuproptosis and glioma biology.

To further explore the clinical implications of this signature, we applied the Tumor Immune Dysfunction and Exclusion (TIDE) algorithm to evaluate predicted responses to immunotherapy across different risk subgroups. The analysis revealed that patients in the low-risk group had lower TIDE scores, suggesting a more favorable immune microenvironment and potentially greater responsiveness to immune checkpoint inhibitors. In contrast, the high-risk group exhibited higher TIDE scores, indicative of increased immune evasion and dysfunction, which may contribute to reduced immunotherapeutic efficacy. These observations suggest a potential association between the lncRNA-based risk signature and immune response in glioma. However, since TIDE is a predictive model based on bulk transcriptomic data, these findings should be interpreted with caution until validated by experimental or clinical data. The results nonetheless provide a computational framework that may assist in identifying patients more likely to benefit from immunotherapy.

We also observed significant differences in drug sensitivity between the high- and low-risk subgroups, particularly with chemotherapy and targeted therapies. While no significant differences were found for temozolomide (TMZ) and EGFR inhibitors between the two subgroups, we identified notable variations in sensitivity to other drugs, such as Bortezomib, Saracatinib, PF-562,271, and AKT inhibitor VIII. High-risk patients showed lower sensitivity to Saracatinib, which may be attributed to a more aggressive TME that promotes drug resistance mechanisms. Conversely, high-risk patients exhibited greater sensitivity to Bortezomib, PF-562,271, and AKT inhibitor VIII, indicating that their tumors may possess a more favorable microenvironment for therapeutic intervention. The association between lower TIDE scores and better responses to these drugs further suggests that a more functional immune system in the low-risk subgroup enhances the effectiveness of these therapies. These results have important implications for personalized treatment strategies. In high-risk patients, however, immune dysfunction and a more resistant TME may necessitate novel treatment strategies, potentially including combination therapies or immune checkpoint inhibitors, to overcome the observed resistance. The use of immune checkpoint inhibitors in high-risk patients may hold promise, though their efficacy will likely depend on overcoming the immune exclusion

mechanisms indicated by the TIDE scores. Moreover, some of the drugs identified, including Bortezomib, Saracatinib, PF-562,271, and AKT inhibitor VIII, have already been tested in clinical trials for glioma, showing varying degrees of success [86–89]. However, their effectiveness is often dependent on the patient's molecular profile. For example, the tumor microenvironment in high-risk glioma patients may influence how well these drugs, particularly AKT inhibitor VIII, exert their therapeutic effects. The next step will involve validating these findings in clinical settings, particularly within the context of clinical trials, to determine how best to integrate these risk stratifications into treatment planning. Such validations are crucial for confirming the potential of TIDE-based risk stratification as a tool for personalizing glioma treatment and ultimately improving patient outcomes.

We also observed differences in predicted drug sensitivity between the high- and low-risk subgroups, particularly in response to several chemotherapy and targeted agents. While no significant differences were predicted for temozolomide (TMZ) and EGFR inhibitors, varying sensitivities were noted for other agents, including Bortezomib, Saracatinib, PF-562,271, and AKT inhibitor VIII. High-risk patients were predicted to exhibit lower sensitivity to Saracatinib, potentially reflecting a more treatment-resistant tumor microenvironment (TME). In contrast, higher predicted sensitivity to Bortezomib, PF-562,271, and AKT inhibitor VIII was observed in the high-risk subgroup, suggesting differential drug response patterns that may relate to underlying molecular characteristics [86–89]. These computational findings, derived using the pRRophetic R package, may inform the development of stratified therapeutic approaches. The association between lower TIDE scores and enhanced predicted sensitivity to certain agents in the low-risk group further suggests that immune function may influence drug efficacy, although this remains to be confirmed experimentally. It is important to note that these predictions are based on in silico models and require validation in biological systems and clinical contexts. Some of the drugs identified—such as Bortezomib, Saracatinib, PF-562,271, and AKT inhibitor VIII—have been previously evaluated in glioma clinical trials with mixed outcomes. Their clinical utility likely depends on patient-specific molecular profiles, including features of the TME. In particular, the efficacy of AKT inhibitor VIII may be modulated by immune infiltration and stromal characteristics, which were not directly assessed in this study. Moving forward, prospective studies and functional assays will be essential to determine the translational value of these predictions. Integration of risk stratification models with experimental validation could support more personalized therapeutic decision-making for glioma patients.

However, there are several limitations to our study. First, although we used data from the TCGA and CGGA cohorts, we did not include verification from other databases such as GEO due to the limitations of commercial microarray sequencing, which hindered the accurate acquisition of lncRNA information. To address this, we randomly divided the cohort into a training group and a validation group for model construction and validation. Furthermore, the potential of the identified lncRNAs as biomarkers has been supported by previous studies. Additionally, we acknowledge that gliomas exhibit significant molecular and spatial heterogeneity, which may limit the accuracy of TIDE scores. Since TIDE scores are based on bulk tumor data, they might not fully capture the immune landscape in distinct tumor regions where immune cell infiltration can vary substantially, potentially affecting the prediction of immune responses. Another

limitation is the lack of experimental validation. While the TIDE score provides useful theoretical predictions based on model data and algorithms, we did not conduct experimental validation (such as immunohistochemistry for immune markers) to confirm the predicted immune responses in glioma samples. This represents an important direction for future studies. Lastly, we did not perform survival analysis due to the limited sample size, but we plan to conduct further validation in future work. Additionally, the specific relationship between the identified lncRNAs and cuproptosis, as well as the detailed mechanisms by which cuproptosis-associated lncRNAs contribute to glioma progression, have not been clearly elucidated in this study. These will be key areas for future research.

11 Conclusion

In conclusion, this study identified ten cuproptosis-related lncRNAs associated with glioma prognosis, providing a basis for risk stratification and the exploration of tumor subtypes. Through computational analyses, we investigated their potential relationships with the immune microenvironment and drug sensitivity, offering insights into possible mechanisms linking cuproptosis to glioma progression. While these findings contribute to understanding the molecular complexity of glioma, they remain hypothesis-generating and require further experimental validation. Future studies are needed to confirm the clinical relevance of these lncRNAs and to elucidate their roles in tumor biology and treatment response.

Supplementary Information

The online version contains supplementary material available at https://doi.org/10.1007/s12672-025-02912-6.

Supplementary Material 1

Supplementary Material 2

Supplementary Material 3

Supplementary Material 4

Supplementary Material 5

Supplementary Material 6

Supplementary Material 7

Supplementary Material 8

Supplementary Material 9

Supplementary Material 10

Acknowledgements

We sincerely thank public databases such as TCGA and CGGA for providing this platform and the investigators for sharing their important data sets.

Author contributions

NDZ and BL designed the implementation of the research, BL, AZ, NDZ and GLY studied and designed all bioinformatics analysis. NDZ, HGW, SC, DBZ, ZYL and BL drafted the preliminary papers. NDZ participated in the investigations. All authors contributed to the article and approved the submitted version.

Funding

No funding.

Data availability

The data of the study are available from supplementary materials or public databases.

Declarations

Ethics approval and consent to participate

This study was approved by the Ethics Committee of Guizhou Provincial People's Hospital. All procedures performed in this study involving human participants were in accordance with the ethical standards of the institutional research committee and with the 1964 Helsinki Declaration and its later amendments.

Consent to publish

All patients provided consent for publication of anonymized data related to this study.

Competing interests

The authors declare no competing interests.

Informed consent

Written informed consent was obtained from all patients involved in the study.

Received: 5 December 2024 / Accepted: 4 June 2025

Published online: 13 June 2025

References

1. Ostrom QT, Price M, Neff C, Cioffi G, Waite KA, Kruchko C, Barnholtz-Sloan JS. CBTRUS statistical report: primary brain and other central nervous system tumors diagnosed in the united States in 2015–2019. Neuro Oncol. 2022;24(Supplement5):v1–95. https://doi.org/10.1093/neuonc/noac202. PMID: 36196752; PMCID: PMC9533228.
2. Komori T. Grading of adult diffuse gliomas according to the 2021 WHO classification of tumors of the central nervous system. Lab Invest. 2022;102(2):126–33. https://doi.org/10.1038/s41374-021-00667-6. PMID: 34504304.
3. Chen J, Han P, Dahiya S. Glioblastoma: Changing concepts in the WHO CNS5 classification. Indian J Pathol Microbiol. 2022;65(Supplement):S24–32. https://doi.org/10.4103/ijpm.ijpm_1109_21. PMID: 35562131.
4. Louis DN, Perry A, Wesseling P, et al. The 2021 WHO classification of tumors of the central nervous system: a summary. Neuro Oncol. 2021;23(8):1231–51. https://doi.org/10.1093/neuonc/noab106.
5. Baumert BG, Hegi ME, van den Bent MJ, et al. Temozolomide chemotherapy versus radiotherapy in high-risk low-grade glioma (EORTC 22033–26033): a randomised, open-label, phase 3 intergroup study. Lancet Oncol. 2016;17(11):1521–32. https://doi.org/10.1016/S1470-2045(16)30313-8.
6. Lapointe S, Perry A, Butowski NA. Primary brain tumours in adults. Lancet. 2018;392(10145):432–46. https://doi.org/10.1016/S0140-6736(18)30990-5.
7. Garcia CR, Slone SA, Dolecek TA, Huang B, Neltner JH, Villano JL. Primary central nervous system tumor treatment and survival in the united states, 2004–2015. J Neurooncol. 2019;144(1):179–91. https://doi.org/10.1007/s11060-019-03218-8.
8. van Solinge TS, Nieland L, Chiocca EA, Broekman MLD. Advances in local therapy for glioblastoma - taking the fight to the tumour. Nat Rev Neurol. 2022;18(4):221–36. https://doi.org/10.1038/s41582-022-00621-0.
9. Xu S, Tang L, Li X, Fan F, Liu Z. Immunotherapy for glioma: current management and future application. Cancer Lett. 2020;476:1–12. https://doi.org/10.1016/j.canlet.2020.02.002.
10. Yang K, Wu Z, Zhang H, et al. Glioma targeted therapy: insight into future of molecular approaches. Mol Cancer. 2022;21(1):39. https://doi.org/10.1186/s12943-022-01513-z.
11. Zhang H, Luo YB, Wu W, et al. The molecular feature of macrophages in tumor immune microenvironment of glioma patients. Comput Struct Biotechnol J. 2021;19:4603–18. https://doi.org/10.1016/j.csbj.2021.08.019.
12. Andersen BM, Faust Akl C, Wheeler MA, Chiocca EA, Reardon DA, Quintana FJ. Glial and myeloid heterogeneity in the brain tumour microenvironment. Nat Rev Cancer. 2021;21(12):786–802. https://doi.org/10.1038/s41568-021-00397-3.
13. Laplane L, Duluc D, Bikfalvi A, Larmonier N, Pradeu T. Beyond the tumour microenvironment [published correction appears in Int J Cancer. 2021;148(6):E5]. Int J Cancer. 2019;145(10):2611–2618. https://doi.org/10.1002/ijc.32343
14. Ma Q, Long W, Xing C, et al. Cancer stem cells and immunosuppressive microenvironment in glioma. Front Immunol. 2018;9:2924. https://doi.org/10.3389/fimmu.2018.02924.
15. Radin DP, Tsirka SE. Interactions between tumor cells, neurons, and microglia in the glioma microenvironment. Int J Mol Sci. 2020;21(22):8476. https://doi.org/10.3390/ijms21228476.
16. Edwardson DW, Parissenti AM, Kovala AT. Chemotherapy and inflammatory cytokine signalling in Cancer cells and the tumour microenvironment. Adv Exp Med Biol. 2019;1152:173–215. https://doi.org/10.1007/978-3-030-20301-6_9.
17. Han S, Liu Y, Cai SJ, et al. IDH mutation in glioma: molecular mechanisms and potential therapeutic targets. Br J Cancer. 2020;122(11):1580–9. https://doi.org/10.1038/s41416-020-0814-x.
18. Rao AM, Quddusi A, Shamim MS. The significance of MGMT methylation in glioblastoma multiforme prognosis. J Pak Med Assoc. 2018;68(7):1137–9.
19. Tesileanu CMS, van den Bent MJ, Sanson M, et al. Prognostic significance of genome-wide DNA methylation profiles within the randomized, phase 3, EORTC CATNON trial on non-1p/19q deleted anaplastic glioma. Neuro Oncol. 2021;23(9):1547–59. https://doi.org/10.1093/neuonc/noab088.
20. Tang D, Kang R, Berghe TV, Vandenabeele P, Kroemer G. The molecular machinery of regulated cell death. Cell Res. 2019;29(5):347–64. https://doi.org/10.1038/s41422-019-0164-5.
21. Tsvetkov P, Coy S, Petrova B et al. Copper induces cell death by targeting lipoylated TCA cycle proteins [published correction appears in Science. 2022;376(6591):eabq4855]. Science. 2022;375(6586):1254–1261. https://doi.org/10.1126/science.abf0529
22. Jian Z, Guo H, Liu H, et al. Oxidative stress, apoptosis and inflammatory responses involved in copper-induced pulmonary toxicity in mice. Aging. 2020;12(17):16867–86. https://doi.org/10.18632/aging.103585.
23. Guo H, Wang Y, Cui H, et al. Copper induces spleen damage through modulation of oxidative stress, apoptosis, DNA damage, and inflammation. Biol Trace Elem Res. 2022;200(2):669–77. https://doi.org/10.1007/s12011-021-02672-8.

24. Kim BE, Nevitt T, Thiele DJ. Mechanisms for copper acquisition, distribution and regulation. Nat Chem Biol. 2008;4(3):176–85. https://doi.org/10.1038/nchembio.72.
25. Scheiber I, Dringen R, Mercer JF. Copper: effects of deficiency and overload. Met Ions Life Sci. 2013;13:359–87. https://doi.org/10.1007/978-94-007-7500-8_11.
26. Kahlson MA, Dixon SJ. Copper-induced cell death. Science. 2022;375(6586):1231–2. https://doi.org/10.1126/science.abo3959.
27. Guo H, Ouyang Y, Yin H, et al. Induction of autophagy via the ROS-dependent AMPK-mTOR pathway protects copper-induced spermatogenesis disorder. Redox Biol. 2022;49:102227. https://doi.org/10.1016/j.redox.2021.102227.
28. Wang X, Zhuang Y, Fang Y, et al. Endoplasmic reticulum stress aggravates copper-induced apoptosis via the PERK/ATF4/CHOP signaling pathway in Duck renal tubular epithelial cells. Environ Pollut. 2021;272:115981. https://doi.org/10.1016/j.envpol.2020.115981.
29. He H, Zou Z, Wang B, et al. Copper oxide nanoparticles induce oxidative DNA damage and cell death via copper Ion-Mediated P38 MAPK activation in vascular endothelial cells. Int J Nanomed. 2020;15:3291–302. https://doi.org/10.2147/IJN.S241157.
30. Hwang JE, de Bruyne M, Warr CG, Burke R. Copper overload and deficiency both adversely affect the central nervous system of Drosophila. Metallomics. 2014;6(12):2223–9. https://doi.org/10.1039/c4mt00140k.
31. Bulcke F, Dringen R, Scheiber IF. Neurotoxicity of copper. Adv Neurobiol. 2017;18:313–43. https://doi.org/10.1007/978-3-319-60189-2_16.
32. Liao J, Yang F, Tang Z, et al. Inhibition of Caspase-1-dependent pyroptosis attenuates copper-induced apoptosis in chicken hepatocytes. Ecotoxicol Environ Saf. 2019;174:110–9. https://doi.org/10.1016/j.ecoenv.2019.02.069.
33. adav P, Sharma P, Sundaram S, Venkatraman G, Bera AK, Karunagaran D. SLC7A11/ xCT is a target of miR-5096 and its restoration partially rescues miR-5096-mediated ferroptosis and anti-tumor effects in human breast cancer cells. Cancer Lett. 2021;522:211–24. https://doi.org/10.1016/j.canlet.2021.09.033.
34. Maher P. Potentiation of glutathione loss and nerve cell death by the transition metals iron and copper: implications for age-related neurodegenerative diseases. Free Radic Biol Med. 2018;115:92–104. https://doi.org/10.1016/j.freeradbiomed.2017.11.015.
35. Li Y, Chen F, Chen J, et al. Disulfiram/Copper induces antitumor activity against both nasopharyngeal Cancer cells and Cancer-Associated fibroblasts through ROS/MAPK and ferroptosis pathways. Cancers (Basel). 2020;12(1):138. https://doi.org/10.3390/cancers12010138.
36. Yang M, Wu X, Hu J, et al. COMMD10 inhibits HIF1α/CP loop to enhance ferroptosis and radiosensitivity by disrupting Cu-Fe balance in hepatocellular carcinoma. J Hepatol. 2022;76(5):1138–50. https://doi.org/10.1016/j.jhep.2022.01.009.
37. Ransohoff JD, Wei Y, Khavari PA. The functions and unique features of long intergenic non-coding RNA. Nat Rev Mol Cell Biol. 2018;19(3):143–57. https://doi.org/10.1038/nrm.2017.104.
38. Sanchez Calle A, Kawamura Y, Yamamoto Y, Takeshita F, Ochiya T. Emerging roles of long non-coding RNA in cancer. Cancer Sci. 2018;109(7):2093–100. https://doi.org/10.1111/cas.13642.
39. Yan H, Bu P. Non-coding RNA in cancer. Essays Biochem. 2021;65(4):625–39. https://doi.org/10.1042/EBC20200032.
40. Zhang X, Zhang W, Jiang Y, Liu K, Ran L, Song F. Identification of functional LncRNAs in gastric cancer by integrative analysis of GEO and TCGA data. J Cell Biochem. 2019;120(10):17898–911. https://doi.org/10.1002/jcb.29058.
41. Li W, Chen QF, Huang T, Wu P, Shen L, Huang ZL. Identification and validation of a prognostic LncRNA signature for hepatocellular carcinoma. Front Oncol. 2020;10:780. https://doi.org/10.3389/fonc.2020.00780.
42. Wu J, Cai Y, Zhao G, Li M. A ten N6-methyladenosine-related long non-coding RNAs signature predicts prognosis of triple-negative breast cancer. J Clin Lab Anal. 2021;35(6):e23779. https://doi.org/10.1002/jcla.23779.
43. Zhao Y, Li MC, Konaté MM et al. TPM, FPKM, or normalized counts? A comparative study of quantification measures for the analysis of RNA-seq data from the NCI patient-derived models repository. *J Transl Med*. 2021;19(1):269. https://doi.org/10.1186/s12967-021-02936-w
44. Leek JT, Johnson WE, Parker HS, Jaffe AE, Storey JD. The Sva package for removing batch effects and other unwanted variation in high-throughput experiments. Bioinformatics. 2012;28(6):882–3. https://doi.org/10.1093/bioinformatics/bts034.
45. Aubert L, Nandagopal N, Steinhart Z, et al. Copper bioavailability is a KRAS-specific vulnerability in colorectal cancer. Nat Commun. 2020;11(1):3701. https://doi.org/10.1038/s41467-020-17549-y.
46. Polishchuk EV, Merolla A, Lichtmannegger J, et al. Activation of autophagy, observed in liver tissues from patients with Wilson disease and from ATP7B-Deficient animals, protects hepatocytes from Copper-Induced apoptosis. Gastroenterology. 2019;156(4):1173–e11895. https://doi.org/10.1053/j.gastro.2018.11.032.
47. Ren X, Li Y, Zhou Y, et al. Overcoming the compensatory elevation of NRF2 renders hepatocellular carcinoma cells more vulnerable to disulfiram/copper-induced ferroptosis. Redox Biol. 2021;46:102122. https://doi.org/10.1016/j.redox.2021.102122.
48. Dong J, Wang X, Xu C et al. Inhibiting NLRP3 inflammasome activation prevents copper-induced neuropathology in a murine model of Wilson's disease. Cell Death Dis. 2021;12(1):87. https://doi.org/10.1038/s41419-021-03397-1
49. Mayakonda A, Lin DC, Assenov Y, Plass C, Koeffler HP. Maftools: efficient and comprehensive analysis of somatic variants in cancer. Genome Res. 2018;28(11):1747–56. https://doi.org/10.1101/gr.239244.118.
50. Ritchie ME, Phipson B, Wu D, et al. Limma powers differential expression analyses for RNA-sequencing and microarray studies. Nucleic Acids Res. 2015;43(7):e47. https://doi.org/10.1093/nar/gkv007.
51. Lossos IS, Czerwinski DK, Alizadeh AA, et al. Prediction of survival in diffuse large-B-cell lymphoma based on the expression of six genes. N Engl J Med. 2004;350(18):1828–37. https://doi.org/10.1056/NEJMoa032520.
52. Alba AC, Agoritsas T, Walsh M, et al. Discrimination and calibration of clinical prediction models: users' guides to the medical literature. JAMA. 2017;318(14):1377–84. https://doi.org/10.1001/jama.2017.12126.
53. Harrell FE Jr, Lee KL, Mark DB. Multivariable prognostic models: issues in developing models, evaluating assumptions and adequacy, and measuring and reducing errors. Stat Med. 1996;15(4):361–87.
54. Ben Salem K, Ben Abdelaziz A. Principal component analysis (PCA). Tunis Med. 2021;99(4):383–9.
55. Chen L, Zhang YH, Wang S, Zhang Y, Huang T, Cai YD. Prediction and analysis of essential genes using the enrichments of gene ontology and KEGG pathways. PLoS ONE. 2017;12(9):e0184129. https://doi.org/10.1371/journal.pone.0184129.
56. Yoshihara K, Shahmoradgoli M, Martínez E, et al. Inferring tumour purity and stromal and immune cell admixture from expression data. Nat Commun. 2013;4:2612. https://doi.org/10.1038/ncomms3612.

57. Subramanian A, Tamayo P, Mootha VK, et al. Gene set enrichment analysis: a knowledge-based approach for interpreting genome-wide expression profiles. Proc Natl Acad Sci U S A. 2005;102(43):15545–50. https://doi.org/10.1073/pnas.0506580102.
58. Brinkman EK, van Steensel B. Rapid quantitative evaluation of CRISPR genome editing by TIDE and TIDER. Methods Mol Biol. 2019;1961:29–44. https://doi.org/10.1007/978-1-4939-9170-9_3.
59. Markouli M, Strepkos D, Papavassiliou KA, Papavassiliou AG, Piperi C. Bivalent genes targeting of glioma heterogeneity and plasticity. Int J Mol Sci. 2021;22(2):540. https://doi.org/10.3390/ijms22020540.
60. Zhou Q, Yan X, Zhu H, et al. Identification of three tumor antigens and immune subtypes for mRNA vaccine development in diffuse glioma. Theranostics. 2021;11(20):9775–90. https://doi.org/10.7150/thno.61677.
61. Zhong H, Liu S, Cao F, et al. Dissecting tumor antigens and immune subtypes of glioma to develop mRNA vaccine. Front Immunol. 2021;12:709986. https://doi.org/10.3389/fimmu.2021.709986.
62. Reifenberger G, Wirsching HG, Knobbe-Thomsen CB, Weller M. Advances in the molecular genetics of gliomas - implications for classification and therapy. Nat Rev Clin Oncol. 2017;14(7):434–52. https://doi.org/10.1038/nrclinonc.2016.204.
63. Song Q, Zhou R, Shu F, Fu W. Cuproptosis scoring system to predict the clinical outcome and immune response in bladder cancer. Front Immunol. 2022;13:958368. https://doi.org/10.3389/fimmu.2022.958368.
64. Liu T, Zhu C, Chen X, et al. Ferroptosis, as the most enriched programmed cell death process in glioma, induces immunosuppression and immunotherapy resistance. Neuro Oncol. 2022;24(7):1113–25. https://doi.org/10.1093/neuonc/noac033.
65. Jakubowicz-Gil J, Bądziul D, Langner E, Wertel I, Zając A, Rzeski W. Temozolomide and Sorafenib as programmed cell death inducers of human glioma cells. Pharmacol Rep. 2017;69(4):779–87. https://doi.org/10.1016/j.pharep.2017.03.008.
66. Obeng E. Apoptosis (programmed cell death) and its signals - A review. Braz J Biol. 2021;81(4):1133–43. https://doi.org/10.1590/1519-6984.228437.
67. Majno G, Joris I. Apoptosis, oncosis, and necrosis. An overview of cell death. Am J Pathol. 1995;146(1):3–15.
68. Guengerich FP. Introduction to metals in biology 2018: copper homeostasis and utilization in redox enzymes. J Biol Chem. 2018;293(13):4603–5. https://doi.org/10.1074/jbc.TM118.002255.
69. Wang H, Shan XQ, Wen B, Zhang S, Wang ZJ. Responses of antioxidative enzymes to accumulation of copper in a copper hyperaccumulator of Commoelina communis. Arch Environ Contam Toxicol. 2004;47(2):185–92. https://doi.org/10.1007/s00244-004-2222-2.
70. Lan QH, Du CC, Yu RJ, et al. Disulfiram-loaded copper sulfide nanoparticles for potential anti-glioma therapy. Int J Pharm. 2021;607:120978. https://doi.org/10.1016/j.ijpharm.2021.120978.
71. Feng S, Liu Y. Metabolomics of glioma. Adv Exp Med Biol. 2021;1280:261–76. https://doi.org/10.1007/978-3-030-51652-9_18.
72. Huang J, Chaudhary R, Cohen AL, et al. A multicenter phase II study of Temozolomide plus Disulfiram and copper for recurrent Temozolomide-resistant glioblastoma. J Neurooncol. 2019;142(3):537–44. https://doi.org/10.1007/s11060-019-03125-y.
73. Xiao K, Peng G. Long non-coding RNA FAM66C regulates glioma growth via the miRNA/LATS1 signaling pathway. Biol Chem. 2021;403(7):679–689. https://doi.org/10.1515/hsz-2021-0333. PMID: 34954927.
74. Lei GL, Li Z, Li YY, Hong ZX, Wang S, Bai ZF, Sun F, Yan J, Yu LX, Yang PH, Yang ZY. Long noncoding RNA FAM66C promotes tumor progression and glycolysis in intrahepatic cholangiocarcinoma by regulating hsa-miR-23b-3p/KCND2 axis. Environ Toxicol. 2021;36(11):2322–2332. https://doi.org/10.1002/tox.23346. Erratum in: Environ Toxicol. 2022;37(2):374. PMID: 34418280.
75. Zhu J, Zhu S, Yu Q, Wu Y. LncRNA FAM66C inhibits pancreatic cancer progression by sponging miR-574-3p. Transl Cancer Res. 2020;9(3):1806–17. https://doi.org/10.21037/tcr.2020.02.24. PMID: 35117528; PMCID: PMC8798657.
76. Xie Y, Gu J, Qin Z, Ren Z, Wang Y, Shi H, Chen B. Long non-coding RNA FAM66C is associated with clinical progression and promotes cell proliferation by inhibiting proteasome pathway in prostate cancer. Cell Biochem Funct. 2020;38(8):1006–16 PMID: 32430927.
77. Wang Y, Zhou W, Ma S, et al. Identification of a Glycolysis-Related LncRNA signature to predict survival in diffuse glioma patients. Front Oncol. 2021;10:597877. https://doi.org/10.3389/fonc.2020.597877.
78. Wang J. Prognostic score model-based signature genes for predicting the prognosis of metastatic skin cutaneous melanoma. Math Biosci Eng. 2021;18(5):5125–45. https://doi.org/10.3934/mbe.2021261.
79. Yang F, Zhao Z, Cai S, et al. Detailed molecular mechanism and potential drugs for COL1A1 in Carboplatin-Resistant ovarian Cancer. Front Oncol. 2021;10:576565. https://doi.org/10.3389/fonc.2020.576565.
80. Huang G, Yang Y, Lv M, et al. Novel LncRNA SFTA1P promotes tumor growth by Down-Regulating miR-4766-5p via PI3K/AKT/mTOR signaling pathway in hepatocellular carcinoma. Onco Targets Ther. 2020;13:9759–70. https://doi.org/10.2147/OTT.S248660.
81. Zheng J, Zhou Z, Qiu Y, et al. A prognostic Ferroptosis-Related LncRNAs signature associated with immune landscape and radiotherapy response in glioma. Front Cell Dev Biol. 2021;9:675555. https://doi.org/10.3389/fcell.2021.675555.
82. Wu F, Zhao Z, Chai R et al. Expression profile analysis of antisense long non-coding RNA identifies WDFY3-AS2 as a prognostic biomarker in diffuse glioma. Cancer Cell Int. 2018;18:107. https://doi.org/10.1186/s12935-018-0603-2
83. Zhou C, Yi C, Yi Y et al. LncRNA PVT1 promotes gemcitabine resistance of pancreatic cancer via activating Wnt/β-catenin and autophagy pathway through modulating the miR-619-5p/Pygo2 and miR-619-5p/ATG14 axes. Mol Cancer. 2020;19(1):118. https://doi.org/10.1186/s12943-020-01237-y
84. Gong R, Li ZQ, Fu K, Ma C, Wang W, Chen JC. Long noncoding RNA PVT1 promotes stemness and Temozolomide resistance through miR-365/ELF4/SOX2 Axis in glioma. Exp Neurobiol. 2021;30(3):244–55. https://doi.org/10.5607/en20060.
85. He Y, Ye Y, Tian W, Qiu H. A novel LncRNA panel related to ferroptosis, tumor progression, and microenvironment is a robust prognostic Indicator for glioma patients. Front Cell Dev Biol. 2021;9:788451. https://doi.org/10.3389/fcell.2021.788451.
86. Tang JH, Yang L, Chen JX, et al. Bortezomib inhibits growth and sensitizes glioma to Temozolomide (TMZ) via down-regulating the FOXM1-Survivin axis. Cancer Commun (Lond). 2019;39(1):81. https://doi.org/10.1186/s40880-019-0424-2.
87. Blomquist MR, Eghlimi R, Beniwal A, et al. EGFRvIII confers sensitivity to Saracatinib in a STAT5-Dependent manner in glioblastoma. Int J Mol Sci. 2024;25(11):6279. https://doi.org/10.3390/ijms25116279.

88. Ortiz-Rivera J, Nuñez R, Kucheryavykh Y, Kucheryavykh L. The PYK2 inhibitor PF-562271 enhances the effect of Temozolomide on tumor growth in a C57Bl/6-Gl261 mouse glioma model. J Neurooncol. 2023;161(3):593–604. https://doi.org/10.1007/s11060-023-04260-3.
89. Cui X, Zhao J, Li G, et al. Blockage of EGFR/AKT and mevalonate pathways synergize the antitumor effect of Temozolomide by reprogramming energy metabolism in glioblastoma. Cancer Commun (Lond). 2023;43(12):1326–53. https://doi.org/10.1002/cac2.12502.

Publisher's note